


Knots and links of polarization singularity lines of light under tight focusing with a parabolic mirror

N. Yu. Kuznetsov, A. E. Ryadchenko, K. S. Grigoriev ^{*}, and V. A. Makarov
Faculty of Physics, Lomonosov Moscow State University, 119991 Moscow, Russia



(Received 24 March 2023; accepted 25 May 2023; published 12 June 2023)

We study topological variations of polarization singularity lines in the electric field of electromagnetic radiation reflected from a parabolic mirror irradiated by elliptically polarized Gaussian and Laguerre-Gaussian beams and two types of Poincaré beams. Torus knots and links of the singular lines of polarization appear as a result of their tight focusing in the reflected radiation. Variation of the polarization ellipticity degree of the Gaussian and Laguerre-Gaussian beams and the parameters defining the polarization distribution of the Poincaré beams causes transformation of the singular lines located near the focal point of the mirror, which is accompanied by a variety of decouplings and reconnections. The total linking number of the singular lines of different types predominantly remains constant upon these reconnections.

DOI: [10.1103/PhysRevA.107.063506](https://doi.org/10.1103/PhysRevA.107.063506)

I. INTRODUCTION

Modern experimental techniques allow us to obtain laser beams with a complex spatial structure of the polarization state. In particular, by virtue of various methods, including spatial spiral phase plates, conical lenses [1] and mirrors [2], holographic masks [3,4], and Pancharatnam-Berry phase optical elements [5,6], light beams with a nontrivial topology of polarization patterns are created. The light field itself is continuous; however, at some points its polarization state does not allow the distribution of the vectors, characterizing the polarization ellipse, to be continuously transformed into a homogeneous one by some class of continuous mappings [7]. Spatial regions with such properties are known as polarization singularities and have attracted considerable interest [8–10] in modern optics. Much attention has been paid to the statistics of the singularities in random fields [10–13] and intentional construction [14–16] of the wave field spatial configurations containing polarization singularities of a given type. However, the description of the topological features of wave fields in many classical problems of even linear optics remains largely understudied.

In recent years three-dimensional distributions of light polarization ellipses in the problems of wave optics with no predominant direction of light propagation have become of particular interest. In this case a number of features can appear in the distribution of the polarization characteristics of the radiation which are fundamentally impossible under the paraxial approximation. Among these structures, which have recently attracted special attention, are phase singularity lines, which form nontrivial knots in space [17–19] and optical Möbius strips [12,13,16,20,21] swept by the polarization ellipse axes as they are traced along a circle.

In this paper we aim to describe the topology of polarization singularity lines of the electric field of the radiation reflected from a parabolic mirror irradiated by elliptically polarized beams with different transverse structure. Particular attention is paid to the knots and links of polarization singularity lines, as well as to the processes of their decoupling and reconnection occurring upon the change of state of polarization of the incident wave.

II. TOPOLOGY OF SINGULAR LINES IN THE NONPARAXIAL FIELD

The electric-field vector \mathcal{E} of an arbitrary monochromatic electromagnetic wave at frequency ω at any point of space given by a radius vector \mathbf{r} changes with time t according to the harmonic law

$$\mathcal{E}(\mathbf{r}, t) = \text{Re}[\mathbf{E}(\mathbf{r}) \exp(-i\omega t)], \quad (1)$$

where \mathbf{E} is the complex amplitude vector of the field. The tip of the vector \mathcal{E} traces an ellipse, the shape and spatial orientation of which can be uniquely specified by four parameters: the intensity $I = |\mathbf{E}|^2$; the degree of ellipticity $M = |\mathbf{E} \times \mathbf{E}^*|/I$, which characterizes the proximity of the ellipse to a circle and takes values from 0 for the case of linear polarization to 1 for a strictly circular polarization; the unit vector normal to the ellipse plane $\mathbf{n} = \text{Im}\{\mathbf{E}^* \times \mathbf{E}\}/I$; and a bidirectional (defined up to a sign change) vector of its major axis $\hat{\mathbf{a}} = \pm \text{Re}\{\mathbf{E}^* \sqrt{(\mathbf{E} \cdot \mathbf{E})}/|\mathbf{E} \cdot \mathbf{E}|\}$.

In general, in a monochromatic fully polarized electromagnetic field, there may be points of polarization singularity at which some of the above characteristics cannot be unambiguously determined. There are two main classes of polarization singularities: C points, where the radiation is circularly polarized (where $M = 1$ and it is impossible to determine the direction of the major axis $\hat{\mathbf{a}}$), and L points, where the radiation is linearly polarized (where $M = 0$ and thus it is impossible to determine the direction of the vector \mathbf{n} normal to

^{*}ksgrigoriev@ilc.edu.ru

the plane of the ellipse). Points of both classes have codimension 2 [22], i.e., their existence is determined by two scalar real independent equations. Circular polarization singularities arise where the real and imaginary parts of the complex vector \mathbf{E} are equal in absolute value and orthogonal, and linear polarization singularities arise where $\text{Re } \mathbf{E}$ and $\text{Im } \mathbf{E}$ have the same or opposite orientation, which has two degrees of freedom in the three-dimensional space. Generically, singularity points in three-dimensional space form structurally stable, isolated nonintersecting curves ($3 - 2 = 1$ dimension), called C lines and L lines for circular and linear cases, respectively. They turn out to be either closed or infinite, i.e., continuing to the boundaries of the investigated area of the electromagnetic field in practice. Near the C (L) lines, the vector $\hat{\mathbf{a}}(\mathbf{n})$ has various orientations, forming topologically nontrivial patterns that can be characterized by the isotropy parameters Υ_C and Υ_L , respectively, taking values from -1 to 1 . A detailed description of the relationship between $\Upsilon_{C,L}$ values and pattern types can be found in [23]. The isotropy parameters coincide in sign with the topological index at every point of the singular lines, but they change continuously along the lines while the topological indices are discrete.

In this paper we describe knots formed by the singularity lines of linear and circular polarization of the electric field in three-dimensional space. Below we will refer to as a knot any simple (having no self-intersections or branches) closed curve in three-dimensional space. A knot can be thought of as a thin elastic thread with its ends closed. Two knots are considered equivalent if one of them can be deformed into the other using a homotopy, i.e., a continuous deformation of the thread from one configuration to another with no intermediary intersections or cuts. A knot is considered trivial if it is equivalent to a circle [24].

Two or more nonintersecting knots form a link. Two links are considered equivalent if they can be mapped onto each other with a homotopy. If a link is equivalent to a countable set of nonintersecting trivial knots (circles) lying in the same plane, it is also called trivial. Two knots are called linked if the link formed by them is nontrivial. Mutual entanglement of a pair of knots is characterized by their linking number. For the case of curves in space, one of its equivalent definitions can be given as follows. First, it is necessary to assign to each of two knots a bypass direction and project them onto an arbitrarily chosen plane such that it contains at most double isolated points of these projections (intersections and self-intersections). Indices $+1$ are assigned to a double point if the contour passing above (in the sense of the chosen projection) intersects the contour passing below from left to right and -1 if the upper contour intersects the lower one from right to left. To the self-intersection points of the projections indices 0 are assigned. The linking number of the contours is half the sum of all the above indices and always takes integer values. It is noteworthy that the value of the linking number does not depend on the choice of the plane of the projection under the above conditions, and the choice of bypass directions affects only the sign of the linking number.

In the general case it is impossible to choose physically interconnected bypass directions for various singular lines; therefore, in this paper we will consider only the absolute

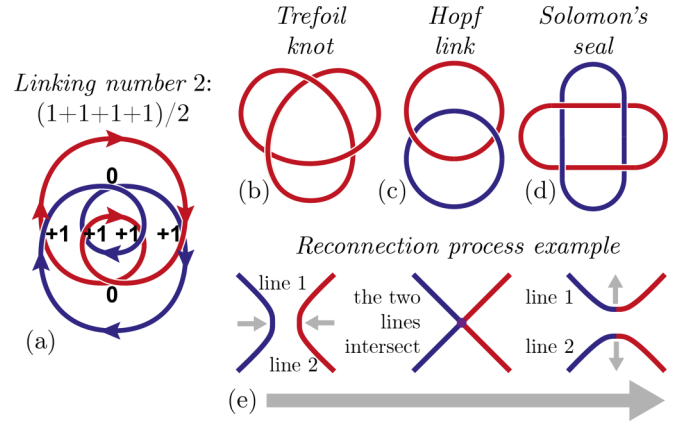


FIG. 1. Examples of the linking number 2 computation of (a) two trivial knots, (b) a trefoil knot, (c) a Hopf link, and (d) Solomon's seal [different realizations in (a) and (d)] and (e) a diagram of the reconnection process.

values of the linking number of such lines. This will affect the calculation of the sum of linking numbers of all the knots in some cases. The linking number is an invariant of a link, that is, it is always the same for equivalent links, but links with the same linking number are not necessarily equivalent. In particular, even knots with zero linking number can be linked. Figure 1(a) shows an example of the linking number (equal to 2) computation for two trivial knots.

Below, the complete set of polarization singularity lines will be referred to as the topological skeleton of the electric field of an electromagnetic wave. Variations of the parameters of the incident radiation, i.e., the medium, optical elements, etc., lead to the movement and deformation of the lines forming it. Possible points of intersection (or self-intersection) of singular lines of the same class have codimension 4 [11] and do not arise in the generic case. However, they can occur in isolation at particular values of a single varied parameter. In this regard, geometric features of the singular lines, caused by the knotting and linking of lines of the same class, are fundamentally removable. When a parameter of the problem varies, the lines can pass through themselves and reconnect. At the same time, an intersection of a C and an L line is possible only at the point of zero intensity ($I = 0$), since it requires simultaneous collinearity and orthogonality of the real and imaginary parts of the vector \mathbf{E} . Points of zero-field intensity have codimension 6 and therefore can be achieved only with simultaneous variation of at least three independent parameters of the problem. Therefore, in most problems with one or even two varied parameters, linking of C lines and L lines with each other remains topologically stable and constitutes a very robust peculiarity of the field structure [11].

All knots encountered in this paper belong to the torus class [25]. In topology an $(m;n)$ -torus knot is a knot that can be completely drawn on a torus. The first of the two coprime integers m and n corresponds to the number of revolutions that the knot makes around the axis of symmetry of the torus and the second (n) corresponds to the number of revolutions around its circular axis. If m and n are not coprime, then

instead of a knot an $(m; n)$ -torus link is formed with $\mathcal{G}(m; n)$ components and linking number [26]

$$l = \frac{m}{2} \left(n - \frac{n}{\mathcal{G}(m; n)} \right) \quad (2)$$

between any two of them. Here \mathcal{G} stands for the greatest common divisor. The most important special cases of torus knots and links are the trefoil knot, which can be represented in the forms of (2; 3)- or (3; 2)-torus knots (topologically equivalent, but with different symmetry) [25] [Fig. 1(b)]; the Hopf link, which is a (2; 2)-torus link with linking number 1 [Fig. 1(c)]; and the (4; 2)-torus link with linking number 2, known as Solomon's seal [Fig. 1(d)]. The link shown in Fig. 1(a) is also equivalent to Solomon's seal, although it looks more complicated.

When a control parameter is changed, two electric-field polarization singularity lines may get closer and then intersect; as a result, their reconnection typically occurs. The latter means that at the point of intersection, these lines break up [red and blue lines in Fig. 1(e)] and the broken parts immediately form another combination of connected components [horizontally oriented two-colored lines in Fig. 1(e)].

It was shown in [23,27] that polarization singularities of both classes can arise as a result of plane monochromatic wave scattering on a subwavelength particle. Two C and one or two L lines linked together with linking number 1 were found in the electric field of radiation reflected from a metal spheroidal particle [23]. In full agreement with the theory developed in [22], such a structure was stable in a wide range of parameters of the incident radiation. At the same time, the topological skeleton of the field, devoid of nontrivial links, in a similar problem of scattering of the same kind of wave by a dielectric particle [27] did not show this level of robustness: L lines in that case were observed only when the polarization of the incident wave was close to linear.

III. PROBLEM STATEMENT

Let an inhomogeneously polarized laser beam propagate along the z axis of the Cartesian coordinate system xyz from the region $z > 0$ and reflect from a concave parabolic mirror with focal and central points on the z axis at coordinates $z = 0$ and $z = -f$, respectively. The electric-field-strength vector of the reflected beam in the vicinity of the geometric focus is calculated using the exact integral solution of Maxwell's equations, obtained in a classical paper [28] for the case of sharp focusing of the incident beam with a parabolic mirror. We have tested the calculation method of the integrals presented in [29,30] by direct comparison of the results of the numerical solution of nonparaxial light propagation equations with exact solutions of Maxwell's equations in a number of problems of linear optics. In the present work we are interested in the electric-field polarization structure in a small neighborhood of the geometric focus. The use of the integral solution [28] of the problem of tight axial focusing of an incident beam by a parabolic mirror in this case leads to lower computational costs compared to the numerical solution of the propagation equations. Numerical simulation has been carried out under conditions reasonably corresponding to the experiment [20]: The laser beam had radius $w = 1$ mm,

wavelength $\lambda = 530$ nm, and focal length $f = 1.128$ mm and the numerical aperture determined from the e^{-2} intensity level was $N_A = 0.9$. Integration of [28] was carried out numerically over the mirror surface from $-5f$ to $5f$ with a resolution of $\Delta x = \Delta y = f/10$. The computational domain was a cube with a side of $4\mu\text{m}$ and the center at the focal point. The resolution along each of the axes of the Cartesian coordinate system was 10 nm.

In the present paper we analyze the features of an elliptically polarized Gaussian beam and Laguerre-Gaussian beams, as well as two varieties of the Poincaré beam, focused by the parabolic mirror described above. The transverse component \mathbf{E}_\perp of the complex amplitude $\mathbf{E} = \mathbf{E}_\perp + \mathbf{E}_\parallel$ of the electric field of the Gaussian beam satisfying the equation $\text{div}\mathbf{E} = 0$ in the plane $z = -f$ is given by

$$\mathbf{E}_\perp(x, y, z = -f) = E_0 \mathbf{e}_0 \exp\left(-\frac{x^2 + y^2}{2w^2}\right), \quad (3)$$

where \mathbf{e} is a unit complex vector

$$\mathbf{e}_0 = (1 - M_0)^{1/2} \mathbf{e}_+ + (1 + M_0)^{1/2} \mathbf{e}_-. \quad (4)$$

In (3) and (4) $\mathbf{e}_\pm = (\mathbf{e}_x \pm i\mathbf{e}_y)/\sqrt{2}$, unit vectors $\mathbf{e}_{x,y}$ are directed along the x and y axes, and E_0 is a real constant. In the paraxial approximation (the longitudinal component $\mathbf{E}_\parallel \approx 0$), the parameter M_0 coincides with the degree of ellipticity $M(x, y)$. The mirror has axial symmetry and without loss of generality we assume that the x axis is parallel to the major axis of the incident radiation polarization ellipse. When the beam is tightly focused, the longitudinal component \mathbf{E}_\parallel of the complex amplitude \mathbf{E} is no longer small and makes a significant contribution to the distribution of the electric-field strength in space [31–33].

The transverse component of the complex amplitude of the Laguerre-Gaussian beam, the intensity of which at the origin is zero and the phase in the immediate vicinity of this point takes all possible values, is given by

$$\mathbf{E}_\perp(x, y, z = -f) = E_0 \mathbf{e}_0 \frac{x \pm iy}{w} \exp\left(-\frac{x^2 + y^2}{2w^2}\right). \quad (5)$$

The beams defined by the opposite signs here are mirror reflections of each other with respect to the $0xz$ plane.

In the waist plane, the transverse component of the complex amplitude of the full Poincaré beam [34] has a more complex form

$$\begin{aligned} \mathbf{E}_\perp(x, y, -f) = E_0 \exp\left(-\frac{x^2 + y^2}{2w^2}\right) \\ \times \left[\mu \mathbf{e}_+ + \left(\frac{p(x + iy) + q(x - iy)}{w} \right) \mathbf{e}_- \right]. \end{aligned} \quad (6)$$

Here E_0 is a real constant and μ is a positive parameter that determines the relative contribution of the circularly polarized Gaussian component to the total electric field equal to $\cot^2 \Theta/2$, using the terminology in [20]. The component of the electric field with opposite circular polarization [the second term in square brackets in (6)] has a phase dislocation [8]. Its type depends on the complex numbers p and q , which can be chosen arbitrarily up to a confinement $|p|^2 + |q|^2 = 1$ and define relative contributions of the Laguerre-Gaussian modes

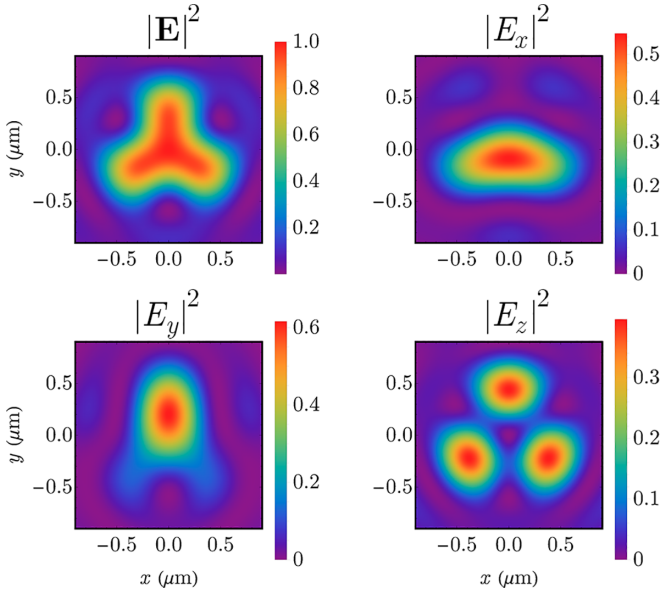


FIG. 2. Distributions of the intensities of the total electric field and its three Cartesian components, obtained in the model of a Poincaré beam with $\mu = 7$, $p = 0$, and $q = 1$.

with opposite helicities of the wavefront. In particular, for the cases of $|p| = 1$ or $|q| = 1$, which are discussed further, the phase dislocation is purely helical; the $p = 1$ and $q = 0$ case here corresponds to $l_2 = 1$ and the $p = 0$ and $q = 1$ case to $l_2 = -1$ in [20]. In the paraxial approximation in the $z = -f$ plane, polarization ellipses of the electric field have all possible aspect ratios and orientations relative to the x axis. At the point $(0, 0, -f)$ the Poincaré beam has purely circular polarization. The isotropy parameter of this singular point is uniquely determined by the values of p and q .

Tight focusing of the star-type Poincaré beam [$p = 0$ and $q = 1$ in Eq. (6)] was studied in [20]. In Fig. 2 the results of our simulation for the total and componentwise field intensities are shown and can be seen to be in good agreement with the results obtained in that paper. In that case the z axis is not only the electric-field polarization singularity line, points of which have the topological index $-1/2$, but also a third-order symmetry axis of the distribution of polarization ellipses under the paraxial approximation. It was shown that around that axis a nontrivial Möbius strip with three half twists is swept out by the $\hat{\mathbf{a}}$ vector as its origin moves along a circle of small radius. Generally, such ribbons are unstable [35] and break up into three fundamental strips with twist coefficients $1/2$. However, a deep analysis of the topological skeleton of the field was not performed in [20] even though it is closely related to the properties of optical Möbius strips.

IV. DISCUSSION OF THE RESULTS

A. Gaussian beam

During the sharp focusing of a Gaussian beam with uniform elliptical polarization (3), only the variation of its initial degree of ellipticity M_0 qualitatively changes the spatial pattern of polarization singularity lines near the focal point of the mirror. When the beam polarization is close to linear, most

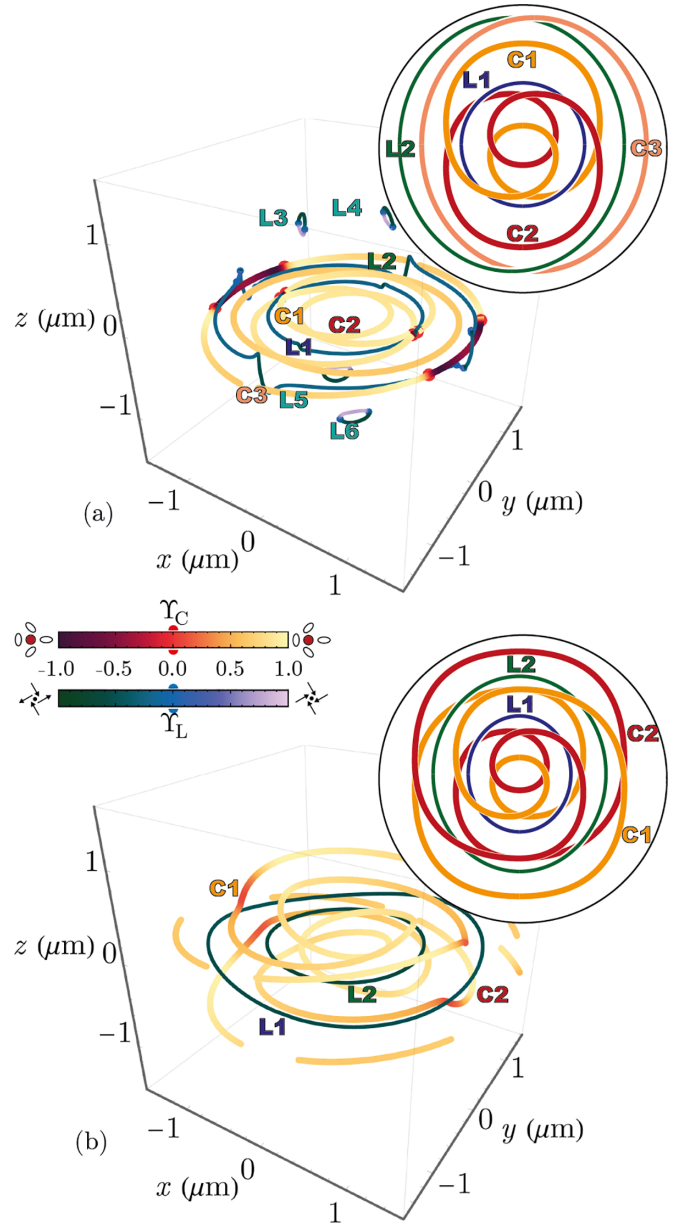


FIG. 3. Topological skeleton of the Gaussian beam tightly focused by a parabolic mirror for (a) $M_0 = 0.05$ and (b) $M_0 = 0.9$. The colors of the lines correspond to the values of the isotropy parameters Υ_C and Υ_L . The round insets depict principal link diagrams with each line in its unique color.

of these lines are located near the $z = 0$ plane. The characteristic topological skeleton of the electric field in this case ($M_0 = 0.05$) is shown in Fig. 3(a). The C and L lines depicted in the figure can be considered as circles slightly deformed in various directions, the centers of which lie close enough to each other near the z axis. The color of the lines corresponds to the value of the isotropy parameters Υ_C and Υ_L of the singular points and small thickenings show the points in space at which the sign of Υ_C and Υ_L (and thus the topological type) changes. Near the color legend, the qualitative distribution of polarization ellipses (for Υ_C) and their normal vectors (for Υ_L) of the light field near the singularity point is shown for the marginal values of the isotropy parameters.

The round inset at the top of Fig. 3(a) shows the fundamental geometry of links of polarization singularity lines in three-dimensional space using a link diagram, i.e., a graphic representation of knots and links in projection onto a plane convenient for their representation, which completely preserves the topology of C and L lines with slight simplifications in their geometry, allowing us to present it most clearly. In order to increase legibility, each of the lines on the link diagram is shown in a characteristic color (except for L3–L6, shown in the same color due to their instability and similarity), and the C lines are thicker than the L lines. It can be seen that the linking number of lines C1 and C2 equals 2 while their shape reflects that of a canonical (2;2)-torus link. Each of these is also linked with the number 1 to the L1 line.

Numerical analysis of the change in the spatial pattern of the electric-field polarization singularity lines with the increase of M_0 allows us to assert that the points of the lines of the same class in the region of their reconnection have opposite signs of the isotropy parameter for all events of this type observed in the present paper. On the contrary, for almost linear polarization of the incident radiation, the values of Υ_C of the points of the C1 and C2 lines in the immediate vicinity of each other are both positive and nearly equal. Therefore, the linking of the polarization singularity lines C1 and C2 is likely to be stable. The line L1 passing between them in a significant part of the link area prevents the reconnections of the above lines with even greater robustness; thus these two lines do not intersect for any value of M_0 .

Lines C3 and L2 in Fig. 3(a) form a Hopf link (linking number 1). It is stable, since it is formed by the two polarization singularity lines of different classes. In this case, the C3 line is divided into four fragments with alternating signs of the isotropy parameter Υ_C . Near the focal plane there are closed curves L3, L4, L5, and L6, not linked to each other or any other lines. As M_0 increases, they shrink and completely disappear at $M_0 = 0.07$, which can be attributed to the triviality of their links since a similar behavior of nonengaged L lines was described in [36] for a scattering problem.

The increase in M_0 also leads to smooth stretching of the circular polarization singularity lines of the reflected radiation along the z axis. Sharp flexures on the L lines characteristic for Fig. 3(a) are smoothed out, and the parameters Υ_C at the points of the C lines become positive everywhere. At $M_0 = 0.87$ the lines C1, C2, and C3 intersect and reconnect. As a result, the outer and inner links combine into a single configuration with the geometry of a (6;2)-torus link. This is clearly seen in Fig. 3(b), constructed for $M_0 = 0.9$. The linking number of the lines C1 and C2 in this case equals 3. Each of them is also separately linked to the lines L1 and L2. In this case, the linking number of each of the four possible combinations of these lines equals 1. The diagram of the described link of the polarization singularity lines is shown in the round inset in Fig. 3(b). Numerical studies allow us to conclude that as M_0 increases, the linking numbers of polarization singularity lines of one class (C lines in the case of $M_0 = 0.9$) change, while the total linking number of C lines with L lines remains constant.

With a further increase in M_0 , the described configuration is destroyed by a cascade of reconnections of C lines with polarization singularity lines lying respectively far from the

mirror focus. As a result, two twisted C line spirals elongated along the z axis are formed, which go beyond the computational domain and apparently stretch to infinity. In this case, the main L lines, the topology of which remains practically the same for any possible M_0 , turn out to be beaded on these spirals. The linking number may not be strictly calculated for the infinite lines, but if naturally reinterpreted as the winding number of the closed line around the elongated one for that case, it still remains constant between the lines of the opposite class.

B. Laguerre-Gaussian beam

As in the preceding section, for an incident Laguerre-Gaussian beam (5), the only parameter qualitatively changing the spatial distribution of the polarization singularity lines of the reflected radiation near the focus of the parabolic mirror is the initial degree of ellipticity M_0 . For $M_0 \leq 0.3$ the structure of C and L lines in the central region of the Laguerre-Gaussian beam is visually very complex: L1 [Fig. 4(a)] and other L lines farther from the z axis not depicted in the figure meander and protrude far beyond the focal region. As M_0 increases, the topological pattern of polarization singularity lines remains unchanged [Figs. 4(b)–4(d)], but the sizes and curvatures of their individual parts change. Closed singular lines (C1, C4, C5, and also L1 when M_0 is larger than approximately 0.5) are located inside the toric region around the z axis. They form a part of the topological skeleton of the electric field of the reflected wave, visually similar to the structure of C and L lines in the case of the incident Gaussian beam (Fig. 3). As before, in these figures the color of the lines corresponds to the values of the isotropy parameters Υ_C and Υ_L , while the L lines are thinner than the C lines.

An important feature of the topological skeleton of the electric field of the reflected wave with the (5) incident beam structure is the presence of polarization singularity lines L2, C2, and C3 extended along the z axis within the focal region [Figs. 4(a)–4(d)], which are depicted as dots on the link diagrams in Figs. 4(e)–4(g). These lines are products of decay of the unstable line of zero intensity of the light field of the incident beam due to the symmetry breaking when the paraxial approximation is no longer valid. The number of these lines is restricted by the requirement of preservation of the total topological index of the incident beam vortex. The isotropy parameter at the points of the C2 and C3 lines is predominantly positive for $M_0 > 0.3$ and predominantly negative for $M_0 < 0.3$. As before, the color of the singular lines in the full images depicts the isotropy parameters and in the link diagrams is unique for each line.

The polarization singularity lines form links that include three closed C lines, C1, C4, and C5, the points of which have predominantly positive isotropy parameter, and one L1 line with predominantly negative values of the isotropy parameter at its points. For all values of M_0 , the total linking number of all closed C lines with the L1 line equals 2. For $M_0 < 0.3$, this is realized due to the linking of C1 and L1 with linking number 2 and the absence of linking between other closed polarization singularity lines. With ellipticity within the range $0.3 < M_0 < 0.8$, this value is achieved by two links with linking numbers 1 between both C lines and the L1 line in

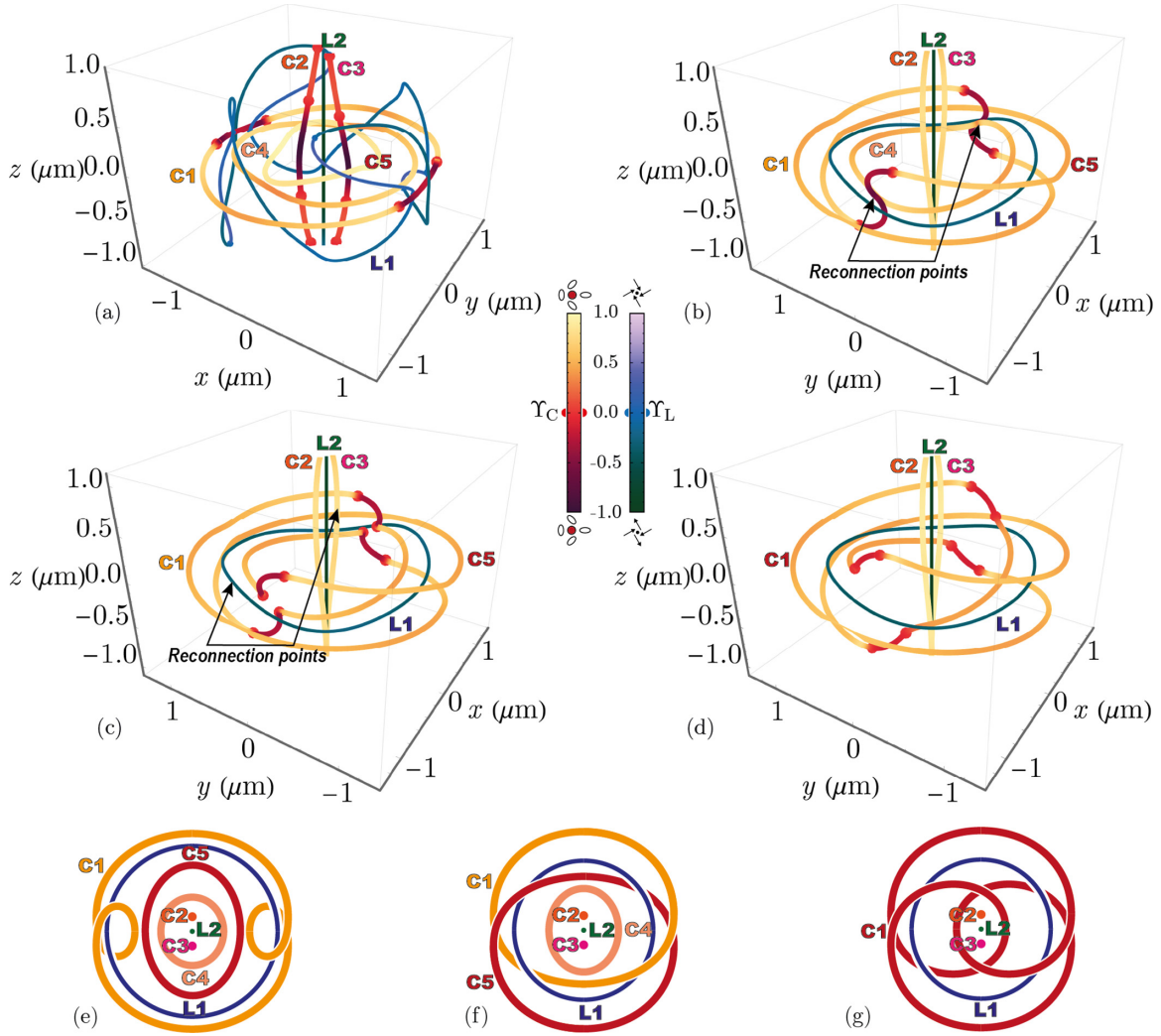


FIG. 4. (a)–(d) Polarization singularity line structures of the reflected radiation and (e)–(g) their link diagrams in the tightly focused Laguerre-Gaussian beam for (a) and (e) $M_0 = 0.25$, (b) and (f) $M_0 = 0.82$, (c) and (f) $M_0 = 0.83$, and (d) and (g) $M_0 = 0.9$.

the absence of a link between lines L1 and C4. Lines C1 and C5 are also linked to each other and each of the infinite lines L2, C2, and C3 is linked to each of the remaining lines in the generalized sense mentioned above. The linking number of all these pairs is 1.

The most noticeable change in the topological skeleton of the electric field of the reflected wave occurs when the polarization of the incident radiation is close to circular. At $M_0 = 0.82$ [Fig. 4(f)] it still resembles the electric-field skeleton typical for $M \approx 0.5$, but there are sharply bent regions on the C1 and C5 lines, the points of which have a negative isotropy parameter. These areas are located close to the C4 line [Fig. 4(b)]. A slight increase in M_0 leads to reconnection of the curves in this region [Fig. 4(c)], which results in the three above-mentioned closed C lines being combined into one, denoted by C1. The latter has the topology of a trefoil knot [Fig. 4(g)] and its geometry is a (3;2)-torus knot representation. Regarding this, the linking number of the knot with the lines C2, C3, and L2 turns out to be equal to 3, i.e., the total linking number of polarization singularity lines stretched along the z axis in the focal region with a set of closed lines that form a knot C1 as a result of reconnection is preserved.

Its linking number with the line L1 is equal to 2 and thus is also preserved. The only linking number undergoing change in some sense is the one between different closed C lines. It equals 0 for small values of M_0 and 1 for the intermediate ones and is undefined for the large ones as there exists only one such line. A further increase of M_0 leads to smoothing of this knot [Fig. 4(d)] and growth of its size. In this case, the line L1 turns into a slightly deformed circle and the lines C2, C3, and L2 practically coincide [Figs. 4(d) and 4(g)].

C. Poincaré beam of the star topological type

Proceeding to the description of the electric-field topological skeleton of the reflected wave of an incident Poincaré beam of the star topological type [$p = 0$ and $q = 1$ in Eq. (6)], we will limit ourselves to the focal point vicinity. In this case we will use the arbitrary amplitude μ of the Gaussian component as a variable parameter. A polarization singularity line C2 exists exactly on its axis for any value of μ and three L lines L2, L3, and L4 can be found close to it for $\mu < 3$. On the link diagrams in Figs. 5 and 6 they are depicted as dots. At the points of all four lines the isotropy parameter is

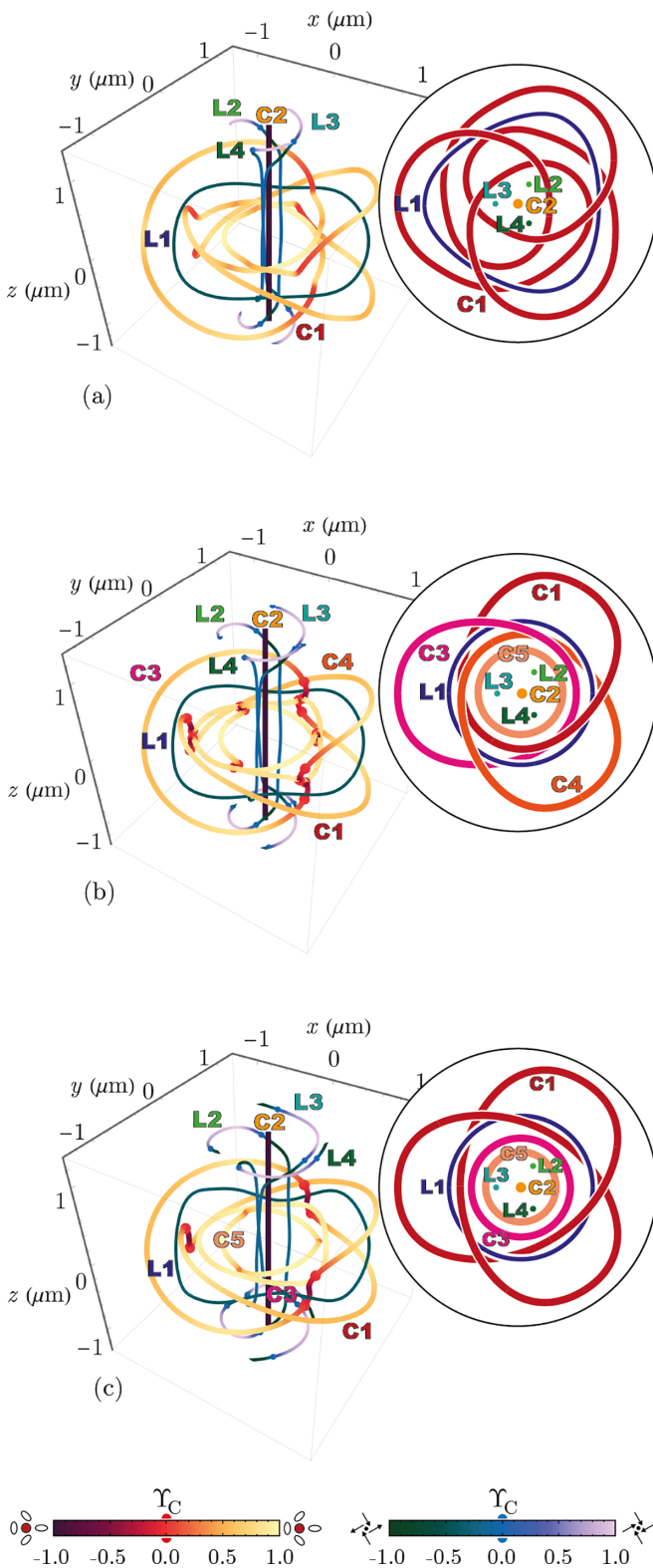


FIG. 5. Central region of the topological skeleton of the light field of a star-type Poincaré beam tightly focused by a parabolic mirror with (a) $\mu = 1$, (b) $\mu = 1.3$, and (c) $\mu = 1.8$. Link diagrams are shown in the round insets with each line depicted in a unique color and L lines thinner than the C lines.

predominantly negative. At about $1 \mu\text{m}$ from the focal plane, the polarization singularity lines twist and acquire a positive isotropy parameter; the larger μ is, the farther they slant from the z axis and the more they deform.

For $\mu \ll 1$, there are also three C lines elongated along the z axis near the lines L2, L3, and L4. As μ increases, they meander, forming pairs of coils oriented towards each other and having opposite signs of the isotropy parameter at their points. As a result, with $\mu \approx 0.87$, the coils separated by the focal plane reconnect and form a polarization singularity line C1, shown in Fig. 5(a) for $\mu = 1$. This line has the topology of a (4; 3)-torus knot, which is additionally linked with linking number 3 to the closed line L1 and with linking number 4 to each of the polarization singularity lines located along the z axis. The latter are also linked to the line L1 (with linking number 1) shaped as a slightly deformed circle.

A further increase of μ is accompanied by a significant complication of the structure of the topological skeleton of the electric field of the reflected wave. At $\mu \approx 1.2$, one more reconnection of the polarization singularity lines occurs; as a result, the C1 line splits into three C lines pairwise linked with linking number 1 [in Fig. 5(b) constructed for $\mu = 1.3$, they are denoted by C1, C3, and C4] and the line C5, which is not linked to any closed line shown in Fig. 5(b). Each of the C1, C3, C4, and C5 lines is also linked to each of the polarization singularity lines C2, L2, L3, and L4 extended along the z axis in the focal region with linking number 1.

With $\mu \approx 1.4$, a new reconnection of the lines shown in Fig. 5(b) takes place. A trefoil knot [in its most famous implementation of the (2; 3)-torus knot] is formed, supplemented by two trivial C lines (C3 and C5). In Fig. 5(c), plotted with $\mu = 1.8$, it is denoted by C1. The knot is linked to the L1 line with linking number 3 and to the infinite lines L2, L3, L4, and C2 with linking number 2. The trivial closed lines L1, C3, and C5 are linked to each of the infinite lines with linking number 1.

We emphasize that in the course of all the reconnections described above, the total linking number between polarization singularity lines of different classes is preserved. In addition, fundamental changes in the topology of polarization singularity lines occur with a minimal change in their geometry because after passing the intersection point, caused by the increase of μ , the C lines move apart by a very small distance compared to the total line length. Before the polarization singularity lines are reconnected, the sign of the isotropy parameter of one of the lines participating in it changes (from positive to negative) near the region of space where the reconnection will occur.

As μ is increased even further (Fig. 6), all C lines, except for C2, without changing their topology, contract towards the focal plane, and disjoint L lines become more elongated along the z axis in the focal region and remote from it in the vicinity of the mirror focus. Farther from the focus, sections of these L lines bend towards the focal plane, and their isotropy parameter changes from negative to positive in these sections, which are shown in purple in Fig. 6(a) ($\mu = 3$). At the same time, ridges almost symmetrical with respect to the focal plane

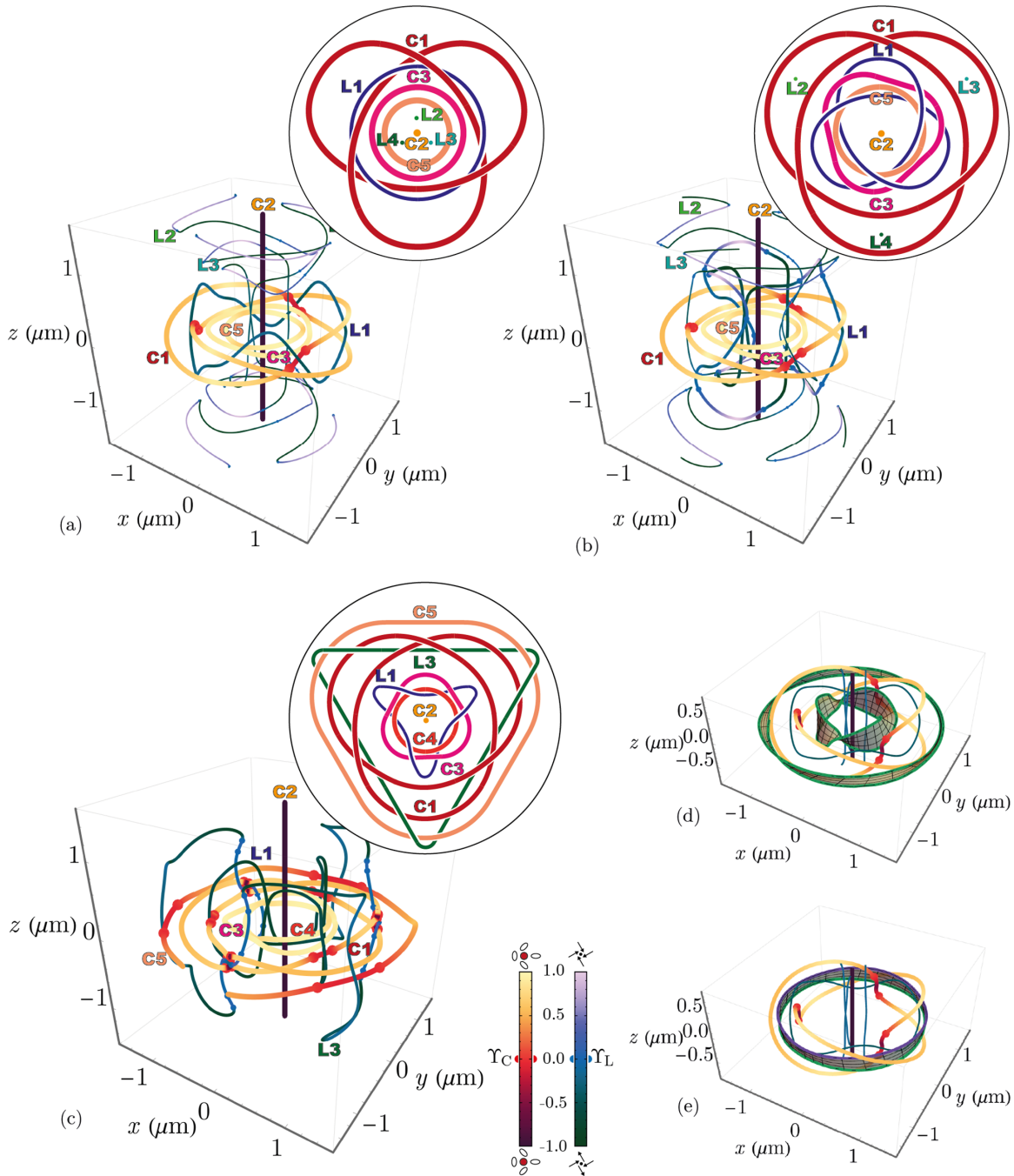


FIG. 6. Central region of the topological skeleton of the light field of a star-type Poincaré beam tightly focused by a parabolic mirror for (a) $\mu = 3$, (b) $\mu = 3.6$, and (c) $\mu = 5$ and principal geometry of the optical strips build along the contours with (d) odd or (e) even linking number with the C-line system. Disjoint L lines are thinner for the sake of legibility. Link diagrams are shown in the round insets.

appear on the closed line L1. As a result, as μ increases, the L lines change in a manner similar to that seen in the C lines dynamics in Fig. 5, and with $\mu \approx 3.3$ they reconnect, forming the L1 trefoil knot shown in Fig. 6(b) plotted with $\mu = 3.6$. It turns out to be linked separately with linking number 3 to the lines C3 and C5, but does not form a link with the knot C1 [see the inset to Fig. 6(b)].

The reconnection at $\mu \approx 3.3$ is the only reconnection we have found that changes the total linking number between lines of different classes. The knot C1, which exists for $\mu < 3.3$, is linked to each of the lines L2, L3, and L4 stretched

along the z axis in the focal region with linking number 2 and to the closed line L1 with linking number 3 [Fig. 5(a)]. In this case, the total linking number is $S_1 = 3 \times 2 + 1 \times 3 = 9$. For $\mu > 3.3$, the knot C1 is linked with linking number 1 to each of the lines L2, L3, and L4 passing through the lugs formed by it (and not its central region) and is not linked to the line L1 [Fig. 5(b)]. As a result, the total linking number becomes lower: $S_2 = 3 \times 1 + 1 \times 0 = 3$.

Such a change must be attributed to the ambiguity in the determination of the bypass directions of the polarization singularity lines and hence the signs of their linking numbers.

Therefore, during the reconnection of two lines of the same class, the linking number can change by a multiple of 2 if the lines participating in it behave as they are oriented oppositely. A star-type Poincaré beam incident on a mirror has a third-order symmetry axis in the distribution of its polarization ellipses. This symmetry requires three lines to simultaneously take part in the reconnection, which leads to a change in the linking number between C1 and L lines under such conditions by the minimum value of 6 admissible both by symmetry and parity. However, the linking number of L lines with the lines C3 and C5 having the trivial topology is equal to 3 and does not change in this case. If, as a result of the reconnection, the linking number of these lines also decreases by 6, it would become equal to -3 . In this case, the new link would turn out to be indistinguishable from the link with number 3 due to the sign indefiniteness mentioned above. The latter can serve as an explanation of the change in the total linking number for one set of lines and its preservation for another one, despite the fact that both of these processes are caused by a change in the geometry of the same polarization singularity lines.

With a relatively large contribution of the Gaussian component to the total strength of the electric field of the beam incident on the mirror ($\mu \approx 3.7$), a new reconnection occurs, resulting in the L knot, shown in Fig. 6(b) splitting into two closed trivial lines L1 and L3 [Fig. 6(c)]. The first of them is individually linked to the lines C3 and C4 with linking number 3 and to the line C2 with linking number 1. The second one (L3) is linked with linking number 3 to the line C1 and a larger trivially closed C line C5, which was not previously part of the same link. The described link, like most of the ones we encountered in this paper, occurs with the conservation of the total linking number of C and L lines, despite the change in their number.

Topologically and symmetrically, the above-described trefoil knots of the electric-field polarization singularity lines completely mirror the edge of an unstable optical Möbius strip with three half twists, swept by a bidirectional vector $\overleftarrow{\mathbf{a}}$ of the major axis of the light polarization ellipse, while it is traced along a circle around the focus in the focal plane. For this vector to sweep the Möbius strip, the tracing contour has to be linked with the C line subsystem of the electric-field topological skeleton with an odd linking number. This condition is satisfied not only for a star-type Poincaré beam in a wide range of μ values, but also for a Laguerre-Gaussian beam and a lemon-type Poincaré beam considered below, but only for a star-type Poincaré beam does such a strip have a knotted edge.

In the focal region of a parabolic mirror, many different twisted and nontwisted strips (ribbons) can be built. The ribbons built near its focus and enclosing only the line C2 coinciding with the z axis have three half twists. Two strips satisfying this condition are shown as an example in Fig. 6(d), also showing the C and L lines lying around them. The color of the latter, as in the previous figures, corresponds to the value of the isotropy parameter at the points of these lines. The ribbons constructed along the contour passing through the knot and having an even linking number l with the polarization singularity lines turn out not to be twisted. One such regular ribbon for $l = 4$ is shown in Fig. 6(e).

D. Poincaré beam of the lemon topological type

In the waist plane, the polarization ellipses distribution of the electric field of a lemon-type Poincaré beam incident on a parabolic mirror [$p = 1$ and $q = 0$ in the expression (6)] does not have axial symmetry. A polarization singularity with the index $+1/2$ exists at the point $(0, 0, -f)$ of that field. These factors combined lead to a very complex singular structure of the field in the nonparaxial case.

For $\mu \ll 1$ in Eq. (6), the topological skeleton of the electric field of the reflected radiation contains a C line extended along the z axis near the focus, next to which there is also an L line folded three times and oriented along the z axis. At a distance from the latter there are also three helical C lines. Finally, for such values of μ , two closed L lines surround the z axis, forming slightly deformed circles. Due to the lack of symmetry in the distribution of polarization ellipses in the incident beam, the isotropy parameters of the C and L lines vary over a wide range while they are traced along the lines.

Starting from $\mu \approx 0.1$, as this parameter grows, the electric-field skeleton described above becomes significantly more complicated, accompanied by a sequence of numerous reconnections and decouplings of polarization singularity lines. Through these, for $\mu = 1.5$, links with linking number 1 are formed between two closed lines of different classes (C and L lines) from a previously existing link between a closed line and an infinite one. Further, the C line of the previously formed link is additionally linked to one more closed C line. This happens for $\mu = 2$, and for $\mu = 3$ these two C lines decouple, but one of them remains linked to the circular L line, confirming the greater topological stability of the links of the different class lines. Another closed C line becomes linked to all the other closed singular lines of the topological skeleton with linking number 1.

A detailed description of all the changes in the pattern of numerous intertwining lines of the electric-field polarization singularity that occur with the increase of μ is hardly possible. Therefore, we confine ourselves to the formulation of the main regularities of the transformation of the topological skeleton of the electric field of the reflected radiation that occurs in this case. First, in those ranges of μ values in which the number of closed polarization singularity lines remains constant, values of the linking coefficients between any two lines of different classes (C and L lines) do not change. Second, if in the course of the reconnections the polarization singularity lines break, then the total linking number of each of the C(L) lines that remained closed with the entire system of L(C) lines is preserved. Disjoint lines must be taken into account during the linking number calculation if they pierce a surface, bounded with a closed one.

This rule is illustrated in Figs. 7(a) and 7(b) plotted, respectively, before ($\mu = 3.5$) and after ($\mu = 4$) the reconnection of the electric-field polarization singularity lines, which occurs at $\mu \approx 3.7$. During the latter, the ring line L1 in Fig. 7(a) opens, connecting with axial lines L2, L3, and L4. The linking numbers of pairs of different class polarization singularity lines of the electric field before and after this reconnection are given in Table I. These numbers are written at the intersections of the rows denoted according to the corresponding C line and the columns denoted according to the corresponding L

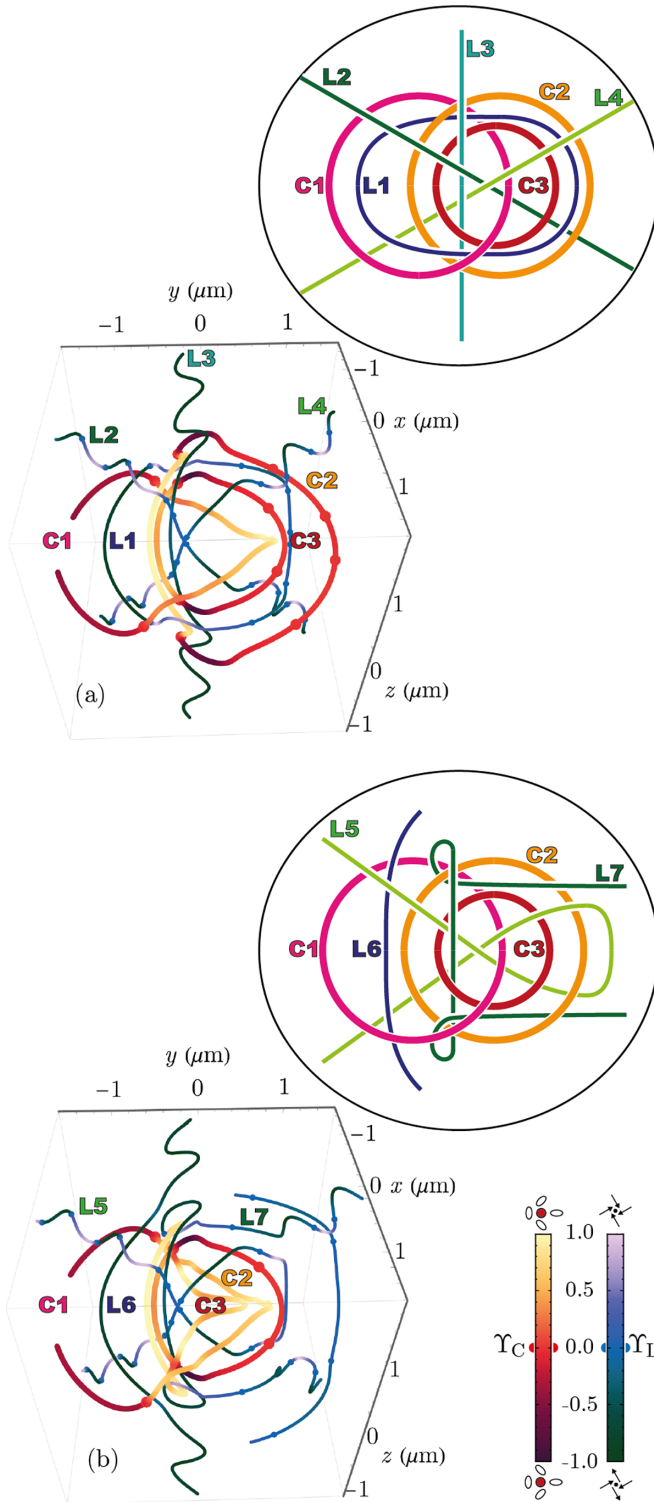


FIG. 7. Central region of the topological skeleton of the light field of a lemon-type Poincaré beam tightly focused by a parabolic mirror with (a) $\mu = 3.5$ and (b) $\mu = 4$. Link diagrams are shown in the round insets with each line depicted in a unique color and L lines thinner than the C lines.

line (L1, L2, L3, and L4 for $\mu = 3.5$) and L5, L6, and L7 for $\mu = 4$. The “sum” columns list the total linking numbers of a specific C line to the whole set of L lines before and

TABLE I. Linking numbers between different classes of singular lines of the electric field of the reflected radiation of a lemon-type Poincaré beam for $\mu = 3.5$ and 4.

Lines	$\mu = 3.5$					$\mu = 4$				
	L1	L2	L3	L4	Sum	L5	L6	L7	Sum	
C1	1	1	1	1	4	C1	2	1	1	4
C2	1	1	1	1	4	C2	2	0	2	4
C3	0	1	1	1	3	C3	2	0	1	3

after the reconnection. It can be seen that not only is the total linking number of all C lines with all L lines preserved (equal to 11 in this case), but also the total linking number of each of the C lines with the whole L line system is preserved since, while the L lines reconnect in this process, the C lines remain topologically intact, though the specific set of the summands in each row changes.

As in the case of a star Poincaré beam, when a Poincaré beam of the lemon type is reflected from the parabolic mirror, one can trace Möbius strips swept by the bidirectional vector \vec{a} near the polarization singularity line while its origin moves along circles of small radius. In this case, they have a single half twist and hence an unknotted edge.

V. CONCLUSION

We have described the topology of polarization singularity lines of the electric field of electromagnetic radiation arising during reflection from a parabolic mirror of elliptically polarized Gaussian and Laguerre-Gaussian beams, as well as two varieties of the Poincaré beam. As a result of their tight focusing ($N_A = 0.9$), three-dimensional topologically nontrivial structures appear in the reflected radiation: knots and links of polarization singularity lines.

If in the waist plane the distribution of polarization ellipses of the transverse component of the electric field of the beam incident on the mirror has an axis of symmetry, then for a wide range of parameters characterizing its polarization, in the reflected radiation near the focus of the mirror there always exists at least one closed L line with the topology of a simple ring, near which the C lines form an $(m; n)$ -torus knot or link, where the numbers m and n are determined by the parameters of the incident beam. This knot (link) is always m -fold linked to the propagation axis of the beams and n -fold linked to the above L line, at which points the electric-field isotropy parameter is always negative.

When the ellipticity degree of the Gaussian and Laguerre-Gaussian beams and the relative amplitudes of circularly polarized components of the Poincaré beam are varied, the topological skeleton of the electric field near the focus is transformed and undergoes a number of decouplings and reconnections of numerous C and L lines. As a rule, near the point in space where a reconnection of polarization singularity lines is expected, they are warped significantly and the isotropy parameter of the singular points, located near the region of further reconnection, takes opposite signs for the two lines (line segments) participating in it. This may limit the possible reconnections of polarization singularity lines in

fields of high symmetry. For almost all polarization states of the beam incident on the mirror, torus knots are formed only by the C lines, the points of which have a predominantly positive isotropy parameter. Also, the numbers m and n characterizing the knot rarely exceed 3. However, for special states of polarization of the Poincaré beam incident on the mirror there exist both more complex knots of the C lines and the knotted L lines (but not simultaneously).

In those ranges of values of the degree of ellipticity of the Gaussian and Laguerre-Gaussian beams and parameters that determine the polarization of the Poincaré beam, in which the number of closed C and L lines in the radiation reflected by the mirror does not change, the values of the linking numbers between any polarization singularity lines of different class remain permanent. The reconnections between different classes of electric-field polarization singularity lines occurring as a result of changes in the distributions of polarization ellipses in the waist plane of the beams incident on the mirror generally demonstrate the conservation of the total linking number between the C and L lines in this process. Rare exceptions to this rule, in which the total linking number changes by an even number as a result of reconnection, is explained by the fact that the linking number for nonoriented curves is determined up to a sign. Also open lines must be taken into account when the linking number is calculated as they were closed at the infinity.

Near the singularity lines of the polarization of the reflected radiation, a large number of optical ribbons may be traced as a

result of movement along closed curves of a vector specifying the direction of the major axis of the electric-field polarization ellipse. Among them, there are ribbons with noninteger values of twists, including Möbius strips, and for the Poincaré beams the topology and symmetry of the edge of these ribbons coincide with the topology and symmetry of the most extended closed C line of the topological skeleton.

A remarkable property of the singular points of the electric-field polarization constituting the topological skeleton is their stability to perturbations. Being predicted on paper, they are very likely to be observed in an experiment as their existence is not subjected to the influence of electromagnetic noises, small inaccuracies of measurement, and so forth. In Ref. [20] optical Möbius strips were successfully observed on the same scale as the key geometric features of the polarization knots and links described in our study have to exist. Therefore, we expect the same experimental techniques to be sufficiently precise to verify the existence of the structures being described in the volume of tightly focused radiation of a light beam with specially designed polarization profile.

ACKNOWLEDGMENTS

The authors are grateful to N. A. Panov, D. E. Shipilo, and I. A. Nikolaeva for their help with numerical calculations and O. G. Kosareva and V. P. Kandidov for useful discussions. This work was supported by the Russian Science Foundation under Grant No. 23-22-00019.

-
- [1] F. Bouchard, H. Mand, M. Mirhosseini, E. Karimi, and R. W. Boyd, Achromatic orbital angular momentum generator, *New J. Phys.* **16**, 123006 (2014).
 - [2] N. Radwell, R. D. Hawley, J. B. Götze, and S. Franke-Arnold, Achromatic vector vortex beams from a glass cone, *Nat. Commun.* **7**, 10564 (2016).
 - [3] F. Cardano, E. Karimi, S. Slussarenko, L. Marrucci, C. de Lisio, and E. Santamato, Polarization pattern of vector vortex beams generated by q -plates with different topological charges, *Appl. Opt.* **51**, C1 (2012).
 - [4] F. Cardano, E. Karimi, L. Marrucci, C. de Lisio, and E. Santamato, Generation and dynamics of optical beams with polarization singularities, *Opt. Express* **21**, 8815 (2013).
 - [5] Z. Bomzon, V. Kleiner, and E. Hasman, Pancharatnam-berry phase in space-variant polarization-state manipulations with subwavelength gratings, *Opt. Lett.* **26**, 1424 (2001).
 - [6] H. Larocque, J. Gagnon-Bischoff, F. Bouchard, R. Fickler, J. Upham, R. W. Boyd, and E. Karimi, Arbitrary optical wavefront shaping via spin-to-orbit coupling, *J. Opt.* **18**, 124002 (2016).
 - [7] O. Y. Viro, O. A. Ivanov, N. Y. Netsvetaev, and V. M. Kharlamov, *Elementary Topology* (American Mathematical Society, Providence, 2008).
 - [8] J. F. Nye, M. V. Berry, and F. C. Frank, Dislocations in wave trains, *Proc. R. Soc. London Ser. A* **336**, 165 (1974).
 - [9] J. F. Nye, *Natural Focusing and Fine Structure of Light: Caustics and Wave Dislocations* (Institute of Physics, Bristol, 1999).
 - [10] M. Dennis, Polarization singularities in paraxial vector fields: Morphology and statistics, *Opt. Commun.* **213**, 201 (2002).
 - [11] L. De Angelis, F. Alpegiani, and L. Kuipers, Spatial Bunching of Same-Index Polarization Singularities in Two-Dimensional Random Vector Waves, *Phys. Rev. X* **8**, 041012 (2018).
 - [12] I. Freund, Optical Möbius strips in three-dimensional ellipse fields: I. Lines of circular polarization, *Opt. Commun.* **283**, 1 (2010).
 - [13] I. Freund, Optical Möbius strips in three dimensional ellipse fields: II. Lines of linear polarization, *Opt. Commun.* **283**, 16 (2010).
 - [14] M. V. Berry and M. R. Dennis, Knotting and unknotting of phase singularities: Helmholtz waves, paraxial waves and waves in $2 + 1$ spacetime, *J. Phys. A: Math. Gen.* **34**, 8877 (2001).
 - [15] M. V. Berry and M. R. Dennis, Knotted and linked phase singularities in monochromatic waves, *Proc. R. Soc. A* **457**, 2251 (2001).
 - [16] I. Freund, Multitwist optical Möbius strips, *Opt. Lett.* **35**, 148 (2010).
 - [17] D. Sugic and M. R. Dennis, Singular knot bundle in light, *J. Opt. Soc. Am. A* **35**, 1987 (2018).
 - [18] H. Larocque, A. D'Errico, M. F. Ferrer-Garcia, A. Carmi, E. Cohen, and E. Karimi, Optical framed knots as information carriers, *Nat. Commun.* **11**, 5119 (2020).
 - [19] J. Zhong, S. Liu, X. Guo, P. Li, B. Wei, L. Han, S. Qi, and J. Zhao, Observation of optical vortex knots and links associated with topological charge, *Opt. Express* **29**, 38849 (2021).
 - [20] T. Bauer, P. Banzer, E. Karimi, S. Orlov, A. Rubano, L. Marrucci, E. Santamato, R. W. Boyd, and G. Leuchs,

- Observation of optical polarization möbius strips, *Science* **347**, 964 (2015).
- [21] E. J. Galvez, I. Dutta, K. Beach, J. J. Zeosky, J. A. Jones, and B. Khajavi, Multitwist Möbius strips and twisted ribbons in the polarization of paraxial light beams, *Sci. Rep.* **7**, 13653 (2017).
- [22] M. Berry and M. Dennis, Polarization singularities in isotropic random vector waves, *Proc. R. Soc. A* **457**, 141 (2001).
- [23] K. S. Grigoriev, N. Y. Kuznetsov, Y. V. Vladimirova, and V. A. Makarov, Fine characteristics of polarization singularities in a three-dimensional electromagnetic field and their properties in the near field of a metallic nanospheroid, *Phys. Rev. A* **98**, 063805 (2018).
- [24] V. V. Prasolov, *Uzly, Zatspleeniia, Kosy i Trekhmernye Mnogobraziiia* (MTsNMO, Moscow, 1997).
- [25] A. Stasiak, V. Katritch, and L. Kauffman, *Ideal Knots* (World Scientific, Singapore, 1998).
- [26] S. Beres, V. Coufal, K. Kearney, R. Lattanzi, and H. Olson, Linking numbers of Klein links, *Coll. Math. J.* **52**, 106 (2021).
- [27] N. Y. Kuznetsov, K. S. Grigoriev, and V. A. Makarov, Topology of polarization-ellipse strips in the light scattered by a dielectric nanosphere, *Phys. Rev. A* **104**, 043505 (2021).
- [28] P. Varga and P. Török, Focusing of electromagnetic waves by paraboloid mirrors. II. Numerical results, *J. Opt. Soc. Am. A* **17**, 2090 (2000).
- [29] A. Couairon, O. G. Kosareva, N. A. Panov, D. E. Shipilo, V. A. Andreeva, V. Jukna, and F. Nesa, Propagation equation for tight-focusing by a parabolic mirror, *Opt. Express* **23**, 31240 (2015).
- [30] D. E. Shipilo, I. A. Nikolaeva, V. Y. Fedorov, S. Tzortzakis, A. Couairon, N. A. Panov, and O. G. Kosareva, Tight focusing of electromagnetic fields by large-aperture mirrors, *Phys. Rev. E* **100**, 033316 (2019).
- [31] B. Richards, E. Wolf, and D. Gabor, Electromagnetic diffraction in optical systems, II. Structure of the image field in an aplanatic system, *Proc. R. Soc. London Ser. A* **253**, 358 (1959).
- [32] H. Kang, B. Jia, and M. Gu, Polarization characterization in the focal volume of high numerical aperture objectives, *Opt. Express* **18**, 10813 (2010).
- [33] X. Xie, L. Li, S. Wang, Z. Wang, and J. Zhou, Three-dimensional measurement of a tightly focused laser beam, *AIP Adv.* **3**, 022110 (2013).
- [34] A. M. Beckley, T. G. Brown, and M. A. Alonso, Full Poincaré beams, *Opt. Express* **18**, 10777 (2010).
- [35] I. Freund, Optical Möbius strips, twisted ribbons, and the index theorem, *Opt. Lett.* **36**, 4506 (2011).
- [36] N. Y. Kuznetsov, K. S. Grigoriev, Y. V. Vladimirova, and V. A. Makarov, Three-dimensional structure of polarization singularities of a light field near a dielectric spherical nanoparticle, *Opt. Express* **28**, 27293 (2020).